Available online at www.sciencedirect.com
ScienceDirect
Journal of the European Ceramic Society 27 (2007) 3253–3259
www.elsevier.com/locate/jeurceramsoc

Room temperature viscosity and delayed elasticity in infrared glass fiber

C. Bernard [a,*], G. Delaizir [b], J.-C. Sangleboeuf [a], V. Keryvin [a], P. Lucas [c], B. Bureau [b], X.-H. Zhang [b], T. Rouxel [a]

[a] *Laboratoire de Recherche en Mécanique Appliquée de l'Université de Rennes 1 (LARMAUR), FRE-CNRS 2717, Campus de Beaulieu, Rennes 35042, France*
[b] *Groupe Verres et Céramiques, UMR-CNRS 6226, Université de Rennes 1, Rennes 35042, France*
[c] *Department of Material Science and Engineering, University of Arizona, 4715 E. Fort Lowell Road, Tucson, AZ 85721, USA*

Received 24 March 2006; received in revised form 21 November 2006; accepted 2 December 2006
Available online 30 January 2007

Abstract

Infrared transparent optical fibers from the Te–As–Se system (TAS) exhibit a viscoelastic behavior at room temperature. The study of the change of the radius of curvature of fibers, once the fibers are unrolled from the mandrel onto which they were rolled just after fiber-drawing, allows the determination of constitutive laws both for the stress relaxation kinetics and for the delayed elasticity process. Whereas, a linear Burger's model provides a good modelling of the stress relaxation stage, a stretched exponential function gives a better description for the delayed elasticity behavior. The room temperature viscosity of the fibers ranges from 3×10^{16} to 2×10^{17} Pa s and the time constant of the anelastic strain recovery process is from 4 to 15 days.

Keywords: Fibers; Creep; Mechanical properties; Glass

1. Introduction

Chalcogenide glasses are of paramount interest for night visibility devices, for medical applications[1–3] or for chemical analyses because of their remarkable transparency in the 3–12 μm range (second atmospheric window). Within chalcogenide glasses, those from the tellurium–arsenic–selenium system (TAS) are very resistant to devitrification and can be drawn into optical fibers which offer exceptional transparency in the mid infrared range. These fibers are used as optical sensors to carry out fiber evanescent wave spectroscopy (so-called FEWS) to investigate, at molecular scale, several problems encountered in microbiology, or environmental protection.[4,5]

The mechanical properties of TAS glasses have been little studied so far.[5,6] Noteworthy, because of their relatively low T_g ranges, these glasses exhibit some viscoelastic effects at room temperature.[6] Preliminary experiments on TAS fibers have shown that, as for Ge–Se glass,[7–9] indentation creep occurs at room temperature, hardness is very low (∼1.4 GPa), and aging treatments in air below T_g induce a dramatic decrease of the tensile strength of the fiber.[6] In this study, the viscoelastic behavior of a TAS glass fiber is investigated by means of fiber bending tests. This kind of test was used by Koide et al.[10] to characterize mechanical relaxation and recovery in silicate glass fibers during an annealing below the glass transition temperature (T_g). In the case of TAS fibers, both stress relaxation, when the fiber is on the mandrel, and change of the radius of curvature, once fibers have been unrolled, occur at room temperature (due to their low glass transition temperature), within a time scale of only a few days for strain changes of 10^{-3}. The amplitude and the kinetics of the rise of the radius of curvature were found to be strongly correlated to the kinetics of the relaxation process occurring when the fibers were still on the rolling mandrel. This phenomenon originates from delayed elasticity and was studied as a function of the time spent on the mandrel as well as the recovery duration after the fiber was unrolled. A constitutive law was determined from the analysis of the data in the light of standard viscoelasticity theory, which further allowed for the prediction of the fiber deformation under service conditions.

* Corresponding author at: LARMAUR, FRE-CNRS 2717, Bat. 10B, Campus de Beaulieu, Université de Rennes 1, 35042 Rennes Cedex, France.
Tel.: +33 2 23 23 62 82; fax: +33 2 23 23 61 11.
E-mail address: cedric.bernard@univ-rennes1.fr (C. Bernard).

0955-2219/$ – see front matter © 2006 Elsevier Ltd. All rights reserved.
doi:10.1016/j.jeurceramsoc.2006.12.001

Table 1
Main properties of the TAS chalcogenide glass

E (GPa)	16.9
T_g (°C) (DSC method)	137
ρ (kg m^{-3})	4.9×10^3
α (°C^{-1})	-270.7×10^{-5}
H (GPa)	1.4

Noteworthy, this glass does not crystallise in standard thermal analysis.

2. Materials and experimental procedures

The fibers were produced from a glass with $Te_2As_3Se_5$ composition. This composition exhibits a wide optical transmission window, from 3 to 12 μm, and an excellent resistance to devitrification during the drawing process avoiding optical scattering losses and keeps good thermomechanical properties (glass transition temperature $T_g = 137$ °C). Raw materials with 99.999 elemental abundance were used for glass preparation as detailed in a previous paper.[11] In order to compensate for the losses due to the further purification, 0.1% of As and 0.2% of Se in mass were added. Selenium and arsenic were purified of remaining oxygen and hydrogen by the volatilization technique by heating them at 240 and 290 °C, respectively under vacuum for several hours. Afterwards, the mixture was distilled and then maintained at 700 °C for 12 h in a rocking furnace to ensure a good homogenization of the liquid. Then the ampoules were quenched in water and annealed near the glass transition temperatures (T_g) to avoid permanent mechanical stresses on cooling. In this manner chalcogenide glass rods were obtained in sizes of about 1 cm diameter and 10 cm length. The as-made composition of the glass was analysed by SEM (JEOL JSM 6301 F) with the energy dispersive spectroscopy method (EDS). And its actual composition after synthesis was (As, Se, and Te) = (29.08, 50.70, and 20.22%), in molar%. The fibers were made from these rods using a drawing tower. Glass cylinders were heated up to the softening temperature, and drawn to the appropriate diameter by selecting the best parameter combination of viscosity and drawing speed. Some physical properties of the studied glasses are given in Table 1. The present investigation was conducted on uncoated fibers in order to avoid any possible influence of the polymer coating on the behavior of the fiber. The diameter of the fibers is about 400 μm.

Fibers were cut in 150 mm long samples which were rolled on a 100 mm diameter mandrel for a maximum of 32 days, and then removed and placed on the smooth and plane surface of a paper grid (see Fig. 1(a)). The change in curvature was continuously monitored by determining the coordinates of three points selected on the fiber. This method leads to a ~5% relative error. All the tests were performed at room temperature: 20 ± 0.5 °C.

Young's modulus, E, and Poisson's ratio, ν, of the glass were determined on a 10 mm thick, 10 mm diameter disk of the glass used for the fiber pre-form, by means of an ultrasonic echography method, from the measurement of the longitudinal (V_l) and transversal (V_t) wave velocities using 10 MHz piezoelectric transducers. E and ν were calculated from the classical elasticity relationships[12]:

$$E = \rho \frac{3V_l^2 - 4V_t^2}{V_l^2/V_t^2 - 1} \quad (1)$$

$$\nu = \frac{3V_l^2 - 4V_t^2}{2(V_l^2 - V_t^2)} - 1 \quad (2)$$

where ρ is the density of the material which was measured at 20 °C by the Archimedean displacement technique using CCl_4 with a relative error of ±0.5%. E and ν are characterized with a better than ±0.5 GPa and 0.01 accuracy (due to experimental error), respectively.

Raman scattering spectrometry was performed on a HR 800 Raman spectrometer using a 632.82 nm wavelength, 13 mW He–Ne laser. The excitation light was focused onto a 1 μm diameter disk region. The scan duration was 60 s with a resolution of 600 lines/mm. The slot thickness was 125 μm, and the confocal hole diameter was 1100 μm. A density filter OD2 was used to divide the power of the laser beam by 100 in order to restrict the temperature rise of the sample.

The viscosity of the glass was measured, above the glass transition temperature, in the range 140–310 °C, by a Rheotronic® parallel plate viscometer (Theta industries, viscosity measurement range: 10^8 to 10^{11} Pa s). The specimen was a 8 mm diameter, 6 mm thick disk of the glass used for the fiber preform. The solver tool of Microsoft® Excel 2000 software was used to fit the experimental curves.

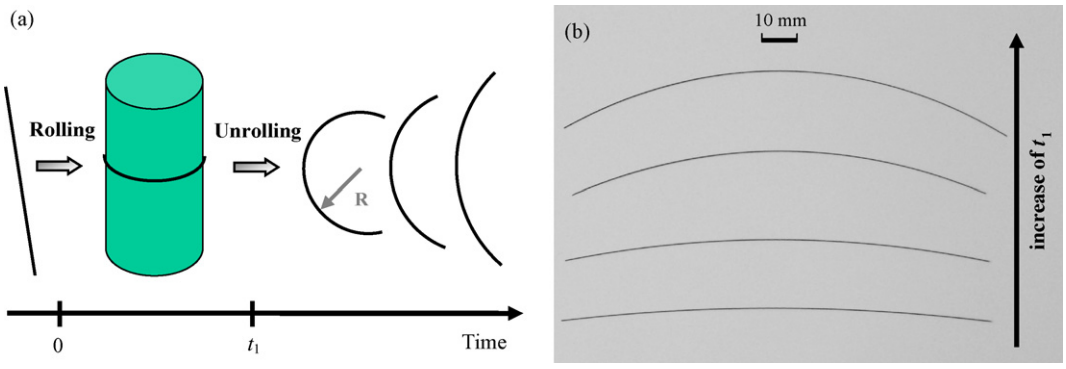

Fig. 1. (a) Chronology of the test: at $t = 0$, a straight fiber is rolled on the mandrel; at $t = t_1$, the fiber is unrolled and the evolution of its radius of curvature, $R(t)$, is measured. (b) Photography of different fibers at the end of the test. Noteworthy, longer the relaxation time, smaller the radius of curvature at the end of the recovery.

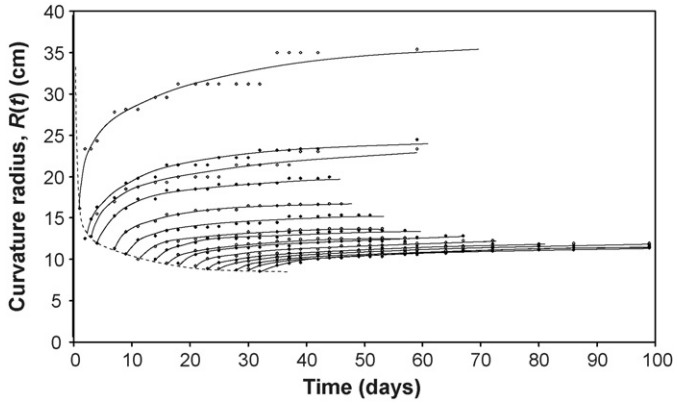

Fig. 2. Time dependence of the curvature radius for different relaxation times t_1 (~5% relative error). The curvature radius just after the instantaneous elastic recovery is represented by the dashed curve.

3. Experimental results and discussion

The change of the radius of curvature of the fibers after unrolling as a function of time is plotted in Fig. 2. The *x*-coordinate of the first point of each recovery curve corresponds to the time the fiber spent on the mandrel (relaxation time). For sake of simplicity and for further use in constitutive laws, we converted the radius of curvature in terms of an apparent strain. The maximum tensile strain in a bent fiber is located on the most external line with respect to the center of curvature (the points for which $y = r$ according to Fig. 3) and is given by $\varepsilon(t) = r/R(t)$, where $R(t)$ is the curvature radius and r the radius of the fiber.[13] The evolution of $\varepsilon(t)$ during the recovery period is plotted in Fig. 4. It is noteworthy that longer the fiber stays on the mandrel, smaller (Fig. 1(b)) and slower the delayed recovery is and smaller the instantaneous elastic recovery is.

The fiber experiences a time-dependent stress, $\sigma(t)$, which is maximum at $t = 0$ ($\sigma = \sigma_0$), i.e., just after being rolled on the mandrel. As illustrated in Fig. 5, while the fiber is around the mandrel, subjected to a constant strain, the associated stress decreases according to a relaxation decay, which could be described by the material relaxation function $\varphi(t)$ as: $\sigma(t) = \sigma_0\varphi(t)$ for $t \in [0,t_1]$. During the delayed elastic recovery of the strain, i.e., after the fiber is unrolled, the fiber curvature radius increases and the

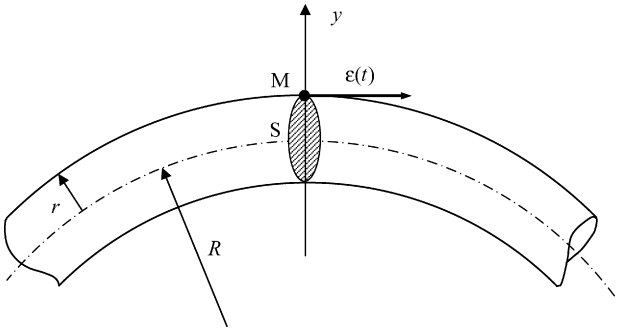

Fig. 3. If the Bernoulli's assumptions are admitted, the maximum value of the tensile strain $\varepsilon(t)$ in one section S of the rolled fiber is reached at the top of the fiber, i.e., at the point M, where r is the radius of the fiber and R its curvature radius.

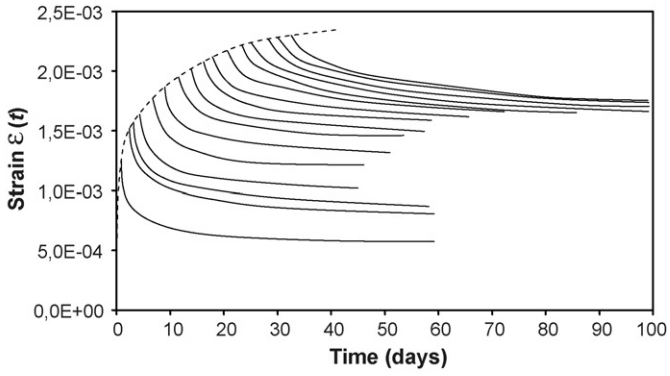

Fig. 4. Time dependence of the maximum strain in the fiber for different relaxation times t_1 (~5% relative error). The maximum strain just after the instantaneous elastic recovery is represented by the dash curve.

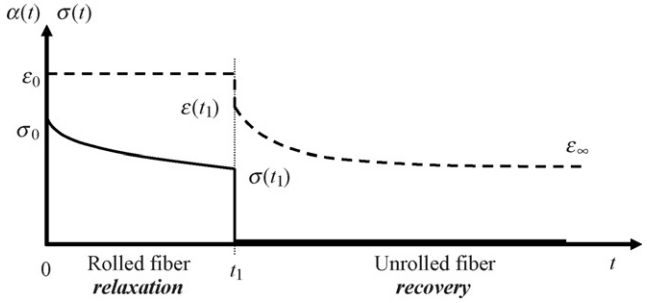

Fig. 5. The time dependence of strain and stress in the fiber during the whole bending test.

corresponding strain is expressed as:

$$\varepsilon(t) = \varepsilon_0 + \varepsilon_{el}(t_1) + \varepsilon_d(t) \quad \text{for } t \in [t_1, \infty],$$

where $\varepsilon_{el}(t_1) = \sigma(t_1)/E$ is the instantaneous elasticity component and ε_d is the delayed elasticity component (anelastic recovery) of the creep compliance (see Fig. 6). Note that $\varepsilon(t)$ tends toward an asymptotic limit, ε_∞, at large time.

The Burger's viscoelastic model, composed of a series combination of Maxwell and Kelvin cells (Fig. 7) provides a simple modelling of the behavior. Four material parameters are introduced, namely: E, the instantaneous elasticity modulus; η, the uniaxial viscosity coefficient; E_d and η_d the parameters of the delayed elasticity part. The simple constitutive equations associated with this model are given in appendix. The instantaneous

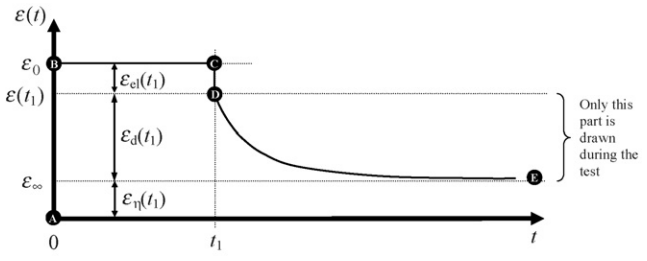

Fig. 6. Different stages of the variation of the strain vs. time. (A–B) Instantaneous elastic strain; (B–C) constant strain; (C–D) instantaneous elastic recovery; (D–E) recovery of the delayed elasticity. Once the test finished, the values of ε_{el}, ε_d, and $\varepsilon_\eta = \varepsilon_\infty$ at time t_1 can be directly measured on the curve.

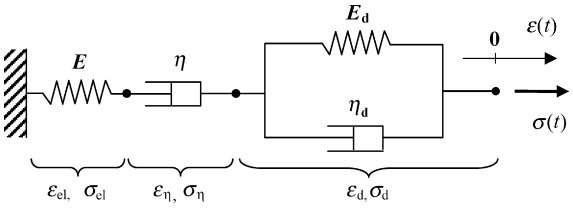

Fig. 7. Uniaxial viscoelastic Burger's model. E is the instantaneous elasticity modulus, η the unrecoverable uniaxial viscosity, E_d and η_d the parameters of the delayed elasticity part, where subscript 'd' stands for delayed elasticity. Note that E is Young's modulus of the glass and η is the viscosity coefficient corresponding to an uniaxial loading ($\eta \approx 2(1+\nu)\eta_{shear}$).

elastic strain just before the unrolling, $\varepsilon_{el}(t_1)$, can be easily measured from the experimental data and is given by: (see schematic drawing Fig. 6)

$$\varepsilon_{el}(t_1) = \varepsilon(t_1) - \varepsilon_0 = \frac{r}{R(t_1)} - \frac{r}{R_0} \tag{3}$$

where R_0 is the mandrel radius.

$\varepsilon_d(t_1)$ and $\varepsilon_\eta(t_1)$ may be evaluated provided the experiment is long enough (aging duration) for an asymptotic limit to show up. Moreover, $\sigma(t_1)$ can be estimated from Hooke's law, $\sigma(t_1) = E\varepsilon_{el}(t_1)$. Since fiber specimens were unloaded from the mandrel at different times t_1, it is possible to draw relaxation curves from all these data for a 32 days duration, and particularly for $\sigma(t)$ (Fig. 8) and $\varepsilon_\eta(t)$ (Fig. 9). Besides, according to the Burger's model, the time dependence of the stress $\sigma(t)$ is given by (see Appendix A):

$$\sigma(t) = \frac{\sigma_0}{\alpha - \beta}\left[\left(\alpha - \frac{E_d}{\eta_d}\right)\exp(-\alpha t) - \left(\beta - \frac{E_d}{\eta_d}\right)\exp(-\beta t)\right] \tag{4}$$

With α and β being the roots of the equation:

$$x^2 - \left(\frac{E}{\eta} + \frac{E}{\eta_d} + \frac{E_d}{\eta_d}\right)x + \frac{EE_d}{\eta\eta_d} = 0 \tag{5}$$

The E value was measured on a bulk glass specimen (fiber preform). The best curve fitting between the experimental relaxation curves $\sigma(t)$ and Eq. (4) is obtained with:

$$\{E,\ \eta,\ E_d,\ \eta_d\} = \{16.9\,\text{GPa},\ \ 1.39\times10^{17}\,\text{Pa s},\ \ 5.51\,\text{GPa},\ \ 6.40\times10^{15}\,\text{Pa s}\}$$

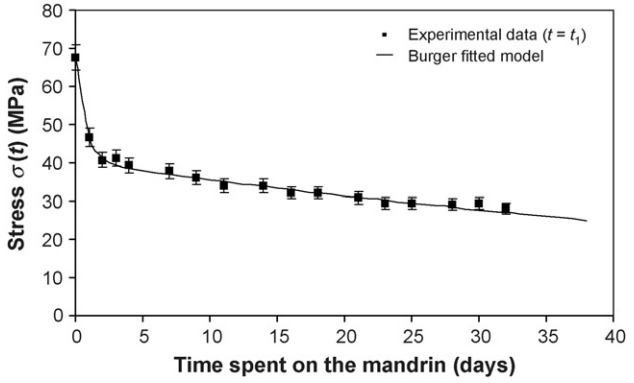

Fig. 8. Time dependence of the stress when the fiber is rolled on the mandrel for the TAS glass (~5% relative error).

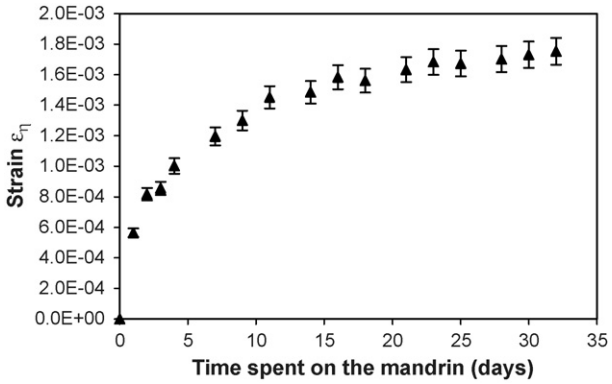

Fig. 9. Time dependence of the dash pot strain during relaxation for the TAS glass (~5% relative error).

The discrepancy between experiment and theory is less than 2% (mean relative error). Moreover, the previously estimated values of $\sigma(t)$ and $\varepsilon_\eta(t)$ allow to estimate an experimental value of η, η_{exp}, according to the relationship:

$$\eta(t) = \frac{\sigma(t)}{\dot{\varepsilon}_\eta(t)} \tag{6}$$

Results presented in Fig. 10 show that the mean value of η_{exp} is about 10^{17} Pa s which is close to the value evaluated with the model, supporting the suitability of the Burger's model for the description of the stress relaxation stage ($t < t_1$). Note that this value would correspond to a time constant, $\tau = \eta/E$, of about 95 days.

Regarding the strain-recovery process, ε_∞ and ε_1 being experimentally available (cf. Fig. 5), the strain evolution after t_1 was modelled with the previously introduced Burger's model. When the parameters of the Burger's model are those determined from the stress relaxation stage, significant differences are observed between the experimental and the theoretical recovery curves (Fig. 11). Indeed, in the beginning of the recovery stage, all the simulated strains rise faster and reach the asymptotic

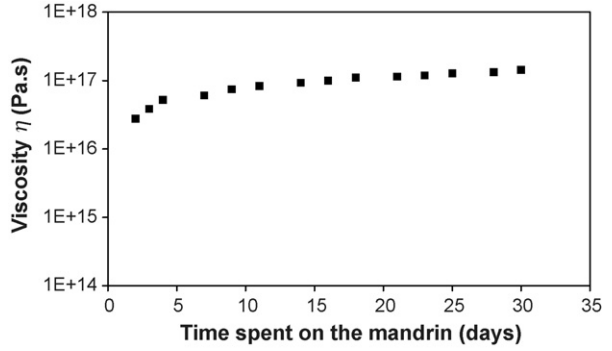

Fig. 10. Viscosity calculated from experimental results vs. time during relaxation for the TAS glass. The mean value after the first days is about 10^{17} Pa s.

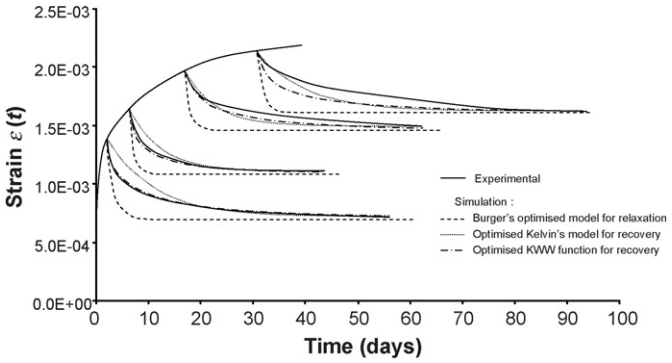

Fig. 11. Comparison of the measured and simulated recovery curves for four different relaxation times.

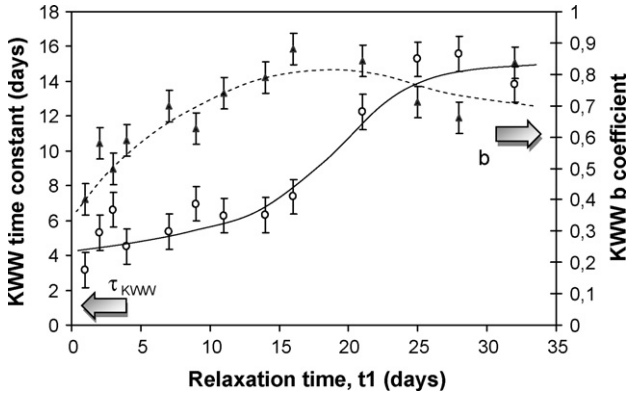

Fig. 12. τ_{KWW} and b parameters of KWW function as a function of time spent on the mandrel.

value sooner than the experimental ones. It means that the characteristic time constant τ_d of the Kelvin cell (the only cell active during the recovery process), defined by: $\tau_d = E_d/\eta_d$, is much lower ($\tau_d = 1.2$ days) than the one of the glass fiber. A single Burger's model is hence unable to predict both the relaxation and the recovery regimes of the fiber. In order to simulate the strain recovery, the Kelvin cell that minimises the gap between all the experimental and calculated values has been determined. This cell is characterized by a time constant: $\tau_d' = 9.5$ days. Fig. 11 shows a relatively good agreement between this model and the experimental data, except for the beginning. Most materials, including inorganic glasses, relax faster than would be expected at the beginning of the relaxation process. De Bast and Gilard[14] and Scherer[15] have shown that the Kohlraush–Williams–Watt (KWW) equation gives a better description in the latter case. This non-linear stretched exponential function (Eq. (6)) shows a very fast kinetics in the beginning.

$$\varepsilon(t) = \varepsilon_\infty \exp\left(-\left(\frac{t}{\tau_{KWW}}\right)^b\right) \quad (7)$$

where b is the stretching parameter ranging from 0 (instantaneous elasticity) to 1, note that for $b = 1$, Eq. (7) reduces to a Kelvin cell equation. The constant time τ_{KWW} is the time needed for the system to reach 66% of its final state.

It is noteworthy that Kurkjian[16] or Gy et al.[17] proposed a generalised Maxwell model, composed of Maxwell cells linked in parallel (six cells for the window glass for example), which proved efficient to model the rheological behavior of a standard float glass at the beginning of the recovery stage. However, this model, which does not reflect more about the physics of the deformation process, introduces many adjustable parameters, and was thus not found attractive in the present case.

Optimisation of b and τ_{KWW} by curve fitting to the recovery curves leads to: $b = 0.57$ and $\tau_{KWW} = 6.6$ days, but as seen in Fig. 11, this couple of values does not involve a suitable simulation after a long relaxation. It highlights that a simple KWW function is not sufficient. Using the same optimisation procedure for every recovery curve (a couple of (τ_{KWW}, b) for each curve) provides a very good description of the recovery behavior whatever the relaxation duration. Indeed, experimental and theoretical curves are almost overlapping (Fig. 11, the relative gap is less than 2%). Moreover, Fig. 12 shows that b and τ_{KWW} values are low for short times spent on the mandrel, which is consistent with the high kinetics observed at the beginning of the recovery part. Further, for long relaxation durations, the slow kinetics of the recovery is nicely modelled by high values of b and τ_{KWW}. Noteworthy, after 15 days relaxation, the value of b is close to 1, meaning that the recovery behavior is nearly the same as that for a single relaxation time viscoelastic model (i.e. Kelvin cell). Finally, the best description for the recovery stage is a KWW function with the changing parameters defined in Fig. 12. Although many authors already used the stretched exponential function to describe the behavior of inorganic glasses, only few studies tried to find a physical understanding for this particular behavior.[18–20] Moreover, these theories have never been experimentally verified. Since we have not enough information about the TAS glass structure to relate the KWW parameters to physical phenomena, we attempted to investigate the material structure.

These results clearly show that the amplitude and the kinetics of the decrease in the strain are strongly correlated to the duration of the relaxation process occurring when the fiber was still on the rolling mandrel. This phenomenon could be explained by a rearrangement of the atomic structure of the glass during the relaxation stage which would modify the behavior of the fiber once it is unrolled. In order to prove such a structural change, Raman scattering spectrometry was used both on an as drawn fiber and on a 6 months relaxed fiber, but the spectra obtained did not show any difference between the two analysed structures. TAS glass is not totally transparent to the red light of the laser (wavelength of 632.82 nm), consequently, a part of the energy is absorbed by the material that leads to a local rise of the temperature. The reached temperature may be high enough to allow the structure to relax locally, i.e., the analysed volume element may have lost its initial structure. Wang et al.[21] investigated the structure of a Se–Ge glass by Raman scattering spectrometry with the same type of laser. The authors kept the temperature rise to under only 3 °C by focusing the laser light onto a large rectangular region (2 mm × 0.2 mm). The power density obtained was 3 W/cm^2. In this study the power density, in spite of the OD2 filter, is about 16 kW/cm^2. As a consequence, the measurements did not characterize the structure of the fibers but the structure of

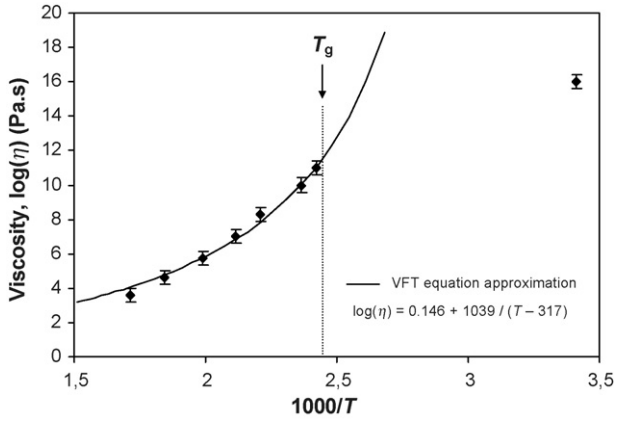

Fig. 13. Viscosity with respect to temperature, and the VFT equation approximation based on high temperature measurements.

the material relaxed by heating. Raman scattering spectrometry with a higher wavelength value or a larger focused region would be more reliable to analyse the structure of TAS glasses.

The viscosity of the TAS glass was measured above T_g (140–310 °C) by a parallel plate viscometer. The results are shown in Fig. 13 and compared with the viscosity measured through the means of the fiber bending test at room temperature. The variation of the viscosity in the vicinity of T_g was approximated by a Vogel–Fulcher–Tamman (VFT) law[22] which is usually used to describe the temperature dependence of glass viscosity: $\log(\eta) = 0.146 + 1039/(T - 44)$). The units of the constants are respectively: $\log(\mathrm{Pa\,s^{-1}})$, $\log(\mathrm{Pa\,s^{-1}})\,^{\circ}\mathrm{C}^{-1}$ and °C. This VFT equation approximation was extrapolated down to room temperature and the large gap between this curve and the experimental value measured at 20 °C, illustrated on Fig. 13, highlights a deviation, below T_g, between the real viscosity variation and the VFT law based on measurements made above glass transition range. This trend, already observed for different kinds of inorganic glasses, can be explained as resulting from the change, with temperature, of the physical mechanisms involved in viscous flow.[23]

4. Conclusion

The viscoelastic behavior of TAS glass fibers has been investigated. Fibers have been rolled during several days on a mandrel and their radius of curvature has been measured continuously after unrolling. It was observed that both amplitude and kinetics of the delayed elastic recovery decrease when relaxation time increases. Optimisation of a Burger's cell leads to a good simulation of the relaxation stage of the fiber. Moreover, the uniaxial viscosity calculated ($\eta \approx 10^{17}$ Pa s) is consistent with the one drawn from the measurements. The recovery period cannot be simulated by a linear viscoelastic model because, on the one hand, it is too fast in kinetics at the beginning and, on the other hand, it is too dependent on the previous relaxation duration time. So, a KWW function in which the b and τ_{KWW} coefficients change as a function of the relaxation time t_1 has been found to be a good means to predict the recovery behavior. The Raman scattering spectrometry we used did not characterize a hypothetic structural rearrangement occurring during relaxation, but a Raman spectrometry with an infrared laser or a larger focused region would bring more reliable information about the atomic scale changes. Finally, viscosity values measured at room temperature using the fiber bending test and those measured above T_g are in agreement with those reported in previous studies concerning other inorganic glasses.

Acknowledgements

The authors gratefully thank A. Moreac for performing Raman spectrometry analyses and for his help. C. Bernard acknowledges the French Ministry of Education and Research for his Ph.D. grant.

Appendix A

Calculation of the evolution of the stress in a Burger's cell during relaxation stage. The constitutive laws of the simple elements composing Burger's cell are:

$$\sigma_{el} = E\varepsilon_{el} \tag{A.1}$$

$$\sigma_{\eta} = \eta\dot{\varepsilon}_{\eta} \tag{A.2}$$

$$\sigma_{d} = E_{d}\varepsilon_{d} + \eta_{d}\dot{\varepsilon}_{d} \tag{A.3}$$

Moreover, the way these cells are linked leads to the following relationships:

$$\varepsilon = \varepsilon_{el} + \varepsilon_{\eta} + \varepsilon_{d} \tag{A.4}$$

$$\sigma = \sigma_{el} = \sigma_{\eta} = \sigma_{d} \tag{A.5}$$

All these notations are defined in Fig. 7.

Differentiating Eq. (A.4) and using Eqs. (A.1)–(A.3), it leads to:

$$\dot{\varepsilon} = \frac{1}{\eta}\sigma + \left(\frac{1}{E} + \frac{1}{E_d}\right)\dot{\sigma} - \frac{\eta_d}{E_d}\ddot{\varepsilon}_d \tag{A.6}$$

$\ddot{\varepsilon}_d$ can be expressed by differentiating twice both Eqs. (A.1) and (A.2), and injecting them in the Eq. (A.4):

$$\ddot{\varepsilon} = \frac{1}{\eta}\dot{\sigma} + \frac{1}{E}\ddot{\sigma} + \ddot{\varepsilon}_d \tag{A.7}$$

$$\ddot{\varepsilon}_d = \ddot{\varepsilon} - \frac{1}{\eta}\dot{\sigma} - \frac{1}{E}\ddot{\sigma} \tag{A.8}$$

The constitutive law of the Burger's model is obtained by substituting $\dot{\varepsilon}_d$, given by Eq. (A.8) in Eq. (A.6):

$$\frac{d}{dt}\left[\frac{\eta_d}{E_d}\dot{\varepsilon} + \varepsilon\right] = \frac{1}{\eta}\sigma + \left[\frac{1}{E} + \frac{1}{E_d} + \frac{\eta_d}{\eta E_d}\right]\dot{\sigma} + \frac{\eta_d}{EE_d}\ddot{\sigma} \tag{A.9}$$

During the relaxation stage, $\dot{\varepsilon}$ remains constant, so Eq. (A.9) becomes:

$$\frac{\eta_d}{EE_d}\ddot{\sigma} + \left[\frac{1}{E} + \frac{1}{E_d} + \frac{\eta_d}{\eta}\frac{1}{E_d}\right]\dot{\sigma} + \frac{1}{\eta}\sigma = 0 \tag{A.10}$$

The solution of this second order differential equation is the following equation:

$$\sigma(t) = \frac{\sigma_0}{\alpha - \beta}\left[\left(\alpha - \frac{E_d}{\eta_d}\right)\exp(-\alpha t) - \left(\beta - \frac{E_d}{\eta_d}\right)\exp(-\beta t)\right] \quad (A.11)$$

where $\sigma_0 = \varepsilon_0 E$, and α and β are the solutions of the subsequent equation:

$$x^2 - \left(\frac{E}{\eta} + \frac{E}{\eta_d} + \frac{E_d}{\eta_d}\right)x + \frac{EE_d}{\eta\eta_d} = 0 \quad (A.12)$$

References

1. Keirsse, J., Boussard-Plédel, C., Loréal, O., Sire, O., Bureau, B., Leroyer, P. *et al.*, IR optical fiber sensor for biomedical applications. *Vib. Spectrosc.*, 2003, **32**, 23–32.
2. Hocdé, S., Loréal, O., Sire, O., Boussard-Plédel, C., Bureau, B., Turlin, B. *et al.*, Metabolic imaging of tissues by infrared fibre-optics spectroscopy: a new approach for medical diagnosis. *J. Biomed. Optic.*, 2004, **9**, 404–407.
3. Lucas, P., LeCoq, D., Junker, C., Collier, J., Boesewetter, D., Boussard, C. *et al.*, Evaluation of toxic agent effects on lung cells by fiber evanescent wave spectroscopy. *Appl. Spectrosc.*, 2005, **59**, 1–9.
4. Michel, K., Bureau, B., Boussard-Plédel, C., Jouan, T., Adam, J. L., Staubmann, K. *et al.*, Monitoring of pollutant in waste water by infrared spectroscopy using chalcogenide glass optical fibers. *Sensor Actuat. B*, 2004, **101**, 252–259.
5. Michel, K., Bureau, B., Boussard-Plédel, C., Jouan, T., Pouvreau, C., Sangleboeuf, J. C. *et al.*, Development of a chalcogenide glass fiber device for in-situ pollutant detection. *J. Non-Cryst. Solids*, 2003, **327**, 434–438.
6. Pouvreau, C., Drissi-Habti, M., Michel, K., Bureau, B., Sangleboeuf, J. C., Boussard-Pledel, C. *et al.*, Mechanical properties of a TAS fiber: a preliminary study. *J. Non-Cryst. Solids*, 2003, **316**, 131–137.
7. Guin, J. P., Rouxel, T., Keryvin, V., Sanglebœuf, J. C., Serre, I. and Lucas, J., Indentation creep of Ge–Se chalcogenide glasses below T_g: elastic recovery and non-Newtonian flow. *J. Non-Cryst. Solids*, 2002, **298**, 260–269.
8. Senapati, U. and Varshneya, A. K., Viscoelasticity of chalcogenide glass-forming liquids: an anomaly in the 'strong' and 'fragile' classification. *J. Non-Cryst. Solids*, 1996, **197**, 210–218.
9. Guin, J. P., Rouxel, T. and Sangleboeuf, J. C., Hardness toughness, and scratchability of germanium–selenium chalcogenide glasses. *J. Am. Ceram. Soc.*, 2002, **85**, 1545–1552.
10. Koide, M., Komatsu, T. and Matusita, K., Delayed elasticity and viscosity of silicate glasses below their glass transition temperature. *Thermochim. Acta*, 1996, **282**, 345–351.
11. Zhang, X. H., Ma, H. L., Blanchetière, C. and Lucas, J., Low loss optical fibres of the tellurium halide-based glasses, the TeX glasses. *J. Non-Cryst. Solids*, 1993, **161**, 327–330.
12. Landau, L. and Lifshitz, E., *Theory of Elasticity (Theoretical Physics, Vol. 7) (3rd ed.)*. Butterworth-Heinemann, 1986.
13. Timoshenko, S., *Strength of Materials. Part 1*. Van Nostrand Reinhold, New York, 1955, Chapter 4.
14. De Bast, J. and Gilard, P., *Comptes rendus de Recherches IRSIA, Vol. 1*. Travaux du centre technique et scientifique de l'industrie belge du verres, 1965, 61 pp. (Chapter 2) [in French].
15. Scherer, G. W., *Relaxation in Glasses and Composites*. John Wiley and Sons Inc., New York, 1986, 45 pp. (Chapter 4).
16. Kurkjian, C. R., *Phys. Chem. Glasses*, 1963, **4**, 128–135.
17. Gy, R., Duffrène, L. and Labrot, M., New insights into the viscoelasticity of glass. *J. Non-Cryst. Solids*, 1994, **175**, 103–117.
18. Trachenko, K. and Dove, M. T., Local event and stretched-exponential relaxation in glass. *Phys. Rev. B*, 2005, **70**, 132202.
19. Ngai, K. L., Temperature dependence of the stretched exponent in structural relaxation of fragile glass-forming molecular liquids. *J. Non-Cryst. Solids*, 1991, **80–83**, 131–133.
20. Palmer, R. G., Stein, D. L., Abrahams, E. and Anderson, P. W., *Phys. Rev. Lett.*, 1984, **53**, 958.
21. Wang, Y., Tanaka, K., Nakaoka, T. and Murase, K., Evidence of nanophase separation in Ge–Se glasses. *J. Non-Cryst. Solids*, 2002, 963–967, 299–302.
22. Fulcher, G., *J. Am. Ceram. Soc.*, 1925, **6**, 339.
23. Shen, J., Green, D. J., Tressler, R. E. and Shelleman, D. L., Stress relaxation of a soda lime silicate glass below the glass transition temperature. *J. Non-Cryst. Solids*, 2003, **324**(3), 277–288.